LASER & PHOTONICS REVIEWS
www.lpr-journal.org

Silicon Programmable Photonic Circuits Based on Periodic Bimodal Waveguides

Luis Torrijos-Morán, Diego Pérez-Galacho, and Daniel Pérez-López*

Programmable photonic circuits are dense assemblies of waveguide meshes in which the flow of light can be reconfigured by software to implement a wide variety of functions, ranging from radiofrequency filtering to optical computing. However, most programmable architectures to date rely on rather bulky Mach-Zehnder interferometers (MZIs), which are not suitable for large-scale and high-density integration. Here, an alternative approach to MZI-based programmable photonic circuits by using slow-light-enhanced periodic bimodal waveguides (PBWs) as programmable units is presented. This study experimentally demonstrates low-loss short tuning elements of 30×1.7 μm^2 in area, achieving a two-orders of magnitude integration density improvement compared to conventional MZIs. A rectangular arrangement of these tunable units is proposed for 3×3 and 4×4 matrix multiplication operations to design a feedforward circuit with a footprint of only 100×250 μm^2. Finally, the performance trade-off and benchmark with alternative programmable unit cells are analyzed in order to address the ever-growing demand for large computing requirements in next-generation applications such as artificial intelligence and quantum information processing.

1. Introduction

Photonic integrated circuits (PICs) have become progressively more important over the last years due to their unique advantages in terms of broad analogue bandwidth, compactness, power consumption, and the possibility of low-cost fabrication.[1–4] These attributes makes PICs attractive for all kind of applications, such as high-speed fiber communications, chemical and biological sensing, metrology, and classical information processing, among others.[5–8] So far, most of PICs are tailored for one specific purpose, the so-called application-specific photonic integrated circuits (ASPICs), given that the flow of light is fixed within a particular circuitry. Nevertheless, these approaches need long design, fabrication, and testing iterations that slows down its development and optimization.[9] Lately, the paradigm of PICs is evolving toward programmable photonic architectures that enable new processing functions and lowers economic and technological barriers.[10–12] The underlying concept of programmable PICs stems from the idea of routing the flow of light through a mesh of waveguides by software control, in order to implement various photonic functions.[13] Toward this end, there has been a growing research effort from both academy and industry in developing general-purpose photonic processors based on programmable waveguide meshes.[14,15] First works on reconfigurable optical devices were reported toward universal linear optics.[16,17] Since then, several experimental demonstrations have been reported on self-configuration using transparent detectors,[18,19] large-scale implementations of up to 26x26 input and output optical ports,[20] and high-speed operation using piezo-optomechanical phase-shifters.[21] A more versatile architecture is achieved using reconfigurable topology meshes, following similar concepts as those employed by Field Programmable Gate Arrays (FPGAs) in electronics.[22] Here, light can be recirculated and enable resonant structures by using triangular, square, and hexagonal shaped meshes.[23–25] These kind of multipurpose processors have demonstrated its flexibility implementing a large variety of functions such as radiofrequency applications, optical beamforming, and sensing, while ensuring self-configuration of large-scale fault-tolerant programmable PICs.[26,27] Programmable circuits can also act as hardware accelerators for matrix multiplication,[28] which are fundamental operations in modern areas such as quantum information processing, neuromorphic computing, and machine learning.[29–33] On this basis, it has been demonstrated years ago that a triangular arrangement of 2×2 photonic structures can be programmed to perform any unitary transformation of a given vector of optical inputs.[34,35] More recently, new designs based on a rectangular arrangements have been proposed with half the optical

L. Torrijos-Morán, D. Pérez-Galacho, D. Pérez-López
Photonics Research Labs
iTEAM Research Institute
Universitat Politècnica de València
Valencia 46022, Spain
E-mail: luis.torrijos@ipronics.com

L. Torrijos-Morán, D. Pérez-López
iPronics Programmable Photonics
Valencia 46010, Spain

D. Pérez-Galacho
Universidad de Málaga, ETSI Telecomunicación
Campus de Teatinos s/n, Málaga 29071, Spain

DOI: 10.1002/lpor.202300505

depth than the previous version and more robust to fabrication errors.[36] Experimental demonstration of rectangular multiport interferometers and different optical implementations have been subsequently reported.[37,38]

In spite of the numerous advantages of programmable PICs, the space utilization of beam splitters and phase shifters restricts the development of large-scale highly integrated circuits.[39] To mitigate some of these limitations, several solutions including phase-change materials (PCMs),[40–42] inversed-design metastructures,[43] or novel photonic arrangements based on diffractive neural networks[44] have been proposed, combined with CMOS-compatible platforms such as silicon-on-insulator (SOI) or silicon nitride technologies.[45,46] In all aforementioned examples, Mach-Zehnder interferometers (MZIs) have become dominant so far as the fundamental building blocks of programmable circuits, thanks in large part to their broadband design, low insertion loss, and tolerance to fabrication errors. However, conventional MZI-based schemes usually require long optical paths that limits its integration in compact footprints and therefore hinders scalability. Alternative approaches that could offer smaller footprint and superior insertion losses could supersede MZI-based structures in the meshes of programmable PICs. Some candidates have recently proposed using multimode interference (MMI) structures, dual-drive directional couplers (DDDCs), and multiport directional couplers (MDCs) as key components to perform unitary optical transformations.[23,47,48] Although they present promising results in terms of robustness to fabrication errors, footprint improvements are not sufficient to replace MZI-based solutions. More compact structures as ring resonators (RRs) and microdisk resonators (MDRs) have also been investigated for programmable photonics,[49] because of their extensive use in switching applications.[50,51] In this case, a compact field-programmable mesh of MDRs is proposed for signal processing functions with remarkable improvements in space utilization.[52]

In parallel, subwavelength-structured waveguides that manipulate light at the nanoscale have reshaped the landscape of PICs as they increase light-matter interaction to drastically boost device performance.[53] This is the case of photonic crystals (PCs), that are especially attractive to generate slow light and enhanced switching operation.[54,55] In this context, 1D periodic waveguides have been reported for several photonic applications,[56] providing a more straightforward and compact design that eases the lithography process, while preserving the slow light benefits typical of PCs. This approach of periodically arranged structures has recently been combined with bimodal configurations[57,58] to develop single-channel interferometers based on periodic bimodal waveguides (PBWs) with an extremely reduced footprint.[59] In addition, PBWs have also been demonstrated as optical switches and sensors in compact devices for the SOI platform.[60,61]

In this work, we explore the use of PBWs as programmable unit cells (PUCs) in an effort to further the progress of high-density integration in programmable PICs. Our approach encompasses the benefits of periodically arranged structures and bimodal waveguides to design extremely short single-channel interferometers for programmable photonics. Here, we design and experimentally validate low-loss and compact silicon PBW-based PUCs capable of performing optical unitary operations. Moreover, we demonstrate 3×3 and 4×4 matrix transformations by implementing a multiport interferometer in a rectangular arrangement with a footprint much more compact than those reported in MZI-based solutions. A comparison of the main findings with other similar works and future perspectives is also provided at the end of the manuscript.

2. Operation Principle and Design

The concept of the proposed programmable photonic mesh built on PBWs is shown in **Figure 1**a for a generalized multiport interferometer of $n \times n$ optical inputs and outputs. Figure 1b corresponds to the actual fabricated device based on a rectangular arrangement of 5 PBWs to implement a 4×4 multiport interferometer. The detailed operation of the PBW-based PUC is depicted in Figure 1c. Light is injected into the PUC through two single-mode waveguides acting as input ports, a_1 and a_2, supporting the fundamental transverse-electric (TE) polarization mode φ_0. The structure is designed so that the fundamental mode of the input waveguide equally excites the first two lower-order modes of the same polarization in the PBW, referred as β_0 and β_1 for the fundamental and the higher order modes, respectively. Similarly, these two modes transfer its power to the fundamental modes φ_0 of the exit waveguides that act as output ports b_1 and b_2. Therefore, 2×2 optical unitary transformations can be performed within the PBW-based PUC by injecting a given vector of optical signals into the input ports. For lossless ideal components, the unitary matrix transfer function can be mathematically written as

$$\begin{bmatrix} b_1 \\ b_2 \end{bmatrix} = \begin{bmatrix} \sqrt{1-\kappa} & i\sqrt{\kappa} \\ i\sqrt{\kappa}e^{i\Delta\Phi} & \sqrt{1-\kappa}e^{i\Delta\Phi} \end{bmatrix} \begin{bmatrix} a_1 \\ a_2 \end{bmatrix} \tag{1}$$

where κ and $\Delta\Phi$ are the power coupling and phase delay of the PUC output signals, respectively. These can be successively expressed as

$$\kappa = \cos^2\left(\frac{\Delta\phi_{\beta_1} - \Delta\phi_{\beta_0}}{2}\right) \tag{2}$$

$$\Delta\Phi = \frac{\Delta\phi_{\beta_1} + \Delta\phi_{\beta_0}}{2} \tag{3}$$

where $\Delta\phi_{\beta_{0,1}}$ refers to the phase shift of the PBW fundamental and high-order mode for a given change in the refractive index of the photonic structure. An electrical heater is placed on top of the PBW to tune the optical response by means of the thermo-optic effect. Note that when an electric current is applied to the heater a phase shift is simultaneously obtained in both modes of the PBW given that they propagate through the same optical path. Nevertheless, this phase shift is not the same for both of them as they are designed to provide different sensitivities to the thermo-optic actuator. This can be achieved by designing the periodic structure so that the modes present a different field distribution along the optical waveguide. In **Figure 2**b, we can see how the optical field of the fundamental mode is confined withing the center of the structure, whereas the high-order mode interacts with the transversal elements (see Note S1, Supporting Information). This fact produces a high-group index contrast between these two modes for a given wavelength range, which can be optimized by

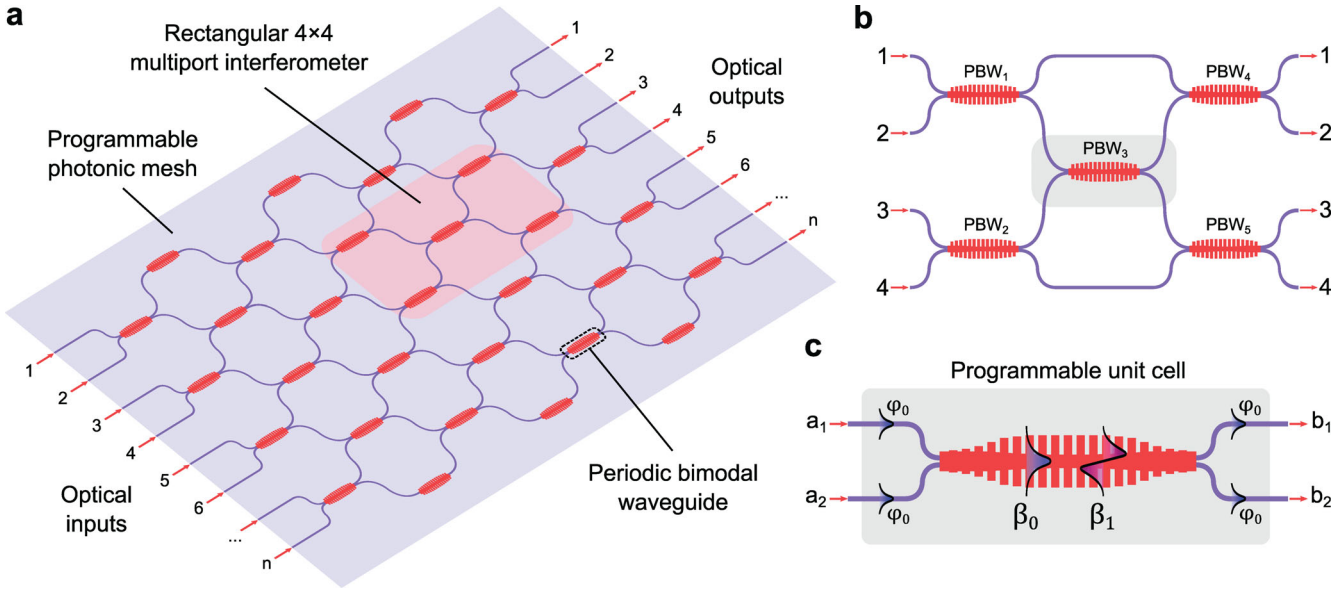

Figure 1. Representation of the proposed concept on programmable photonic circuits using PBWs. a) Sketch of a generic feedforward PBW-based mesh of *n* optical inputs and outputs. b) Schematic of the PBW-based rectangular 4×4 multiport interferometer fabricated to perform unitary matrix multiplication. c) Detailed description of the behavior of a PBW working as a PUC.

properly engineering the band structure for the first even and odd parity modes in the periodic unit cell.[60] As a result, a modal phase shift difference $\Delta\phi_{\beta_1} - \Delta\phi_{\beta_0}$ is produced between the PBW modes, thus enabling the tuning of the power coupling κ for any combination from bar to cross states. To control the phase delay $\Delta\Phi$ of the PUC, another PBW design in which both modes have the same sensitivity must be placed next to the first one (see Note S2, Supporting Information). However, in this article, we focus on the power coupling control to demonstrate, as a proof of concept, a PBW-based programmable PIC for matrix transformations.

The PBW-based PUC design is detailed in Figure 2a. It consists of the following constitutive elements: single-mode waveguide width $w_s = 450$ nm, uniform bimodal width $w = 1000$ nm, mode splitter length $L = 1.5$ µm, PBW periodicity $a = 370$ nm, central PBW element width $w_p = 650$ nm, transversal PBW element length $w_e = 1700$ nm and transversal PBW element width $w_i = 220$ nm. Plain wave expansion (PWE) simulations using MIT Photonic Band (MPB) software have been carried out to numerically obtain the group index. The PBW is designed to exhibit a large group index for the high-order mode compare to the fundamental one (see Figure 2b), in order to enhance the optical efficiency and therefore reduce the length required to ensure a complete modulation transition between bar and cross states. The periodic unit cell dimensions are the same as the one designed in [60]. However, insertion losses reported there were about 2 dBs, which is not suitable for programmable photonic applications. Here we design a new taper at the interface between the single-mode and bimodal parts to reduce losses originating in different sections of the PBW. This taper is formed by the mode splitter and the mode adapter. The former is an uniform bimodal waveguide designed to excite, with a 50:50 split ratio, the first two lower-order modes that will propagate through the periodic waveguide. Next, the mode adapter introduces the periodicity in the photonic structure and gradually adapts the low group index in the uniform bimodal waveguide to the high group index in the PBW. The colormap depicted in Figure 2c shows the design path that must be addressed by the mode adapter, from the starting point (homogeneous width of $w = 1000$ nm) to the ending point ($w_p = 650$ nm and a $w_e = 1700$ nm). Note that the group index increases non-linearly as we reach the ending point so the dimensions of each taper element must be carefully chosen to adapt the group index difference. The number of taper elements has been set to $N_{taper} = 20$ and their dimensions are detailed with purple points in Figure 2c. An exponential evolution of the points has been designed to properly adapt the group index, and thereby avoid modal reflections while achieving low-loss transmission in the PBW (see Note S3, Supporting Information). Finally, the number of elements in the high-group index periodic part has been chosen to be $N = 40$, which corresponds to a PBW total length of 30 µm.

3. Experimental Results

The fabricated programmable chip based on PBWs is shown in **Figure 3**a. A zoomed view of the 4×4 multiport interferometer with a footprint of 100×250 µm^2 is also displayed. The chip has been sent to Advanced Micro Foundry (AMF) for fabrication in 220-nm thick SOI wafers using deep ultraviolet lithography processes. Heaters of 2 µm width have been placed on top of the PBWs, connected to square metal electrodes for the thermo-optical actuation. Small thermal-isolation trenches have been designed close to the PBWs to prevent cross-talk effects. Grating couplers have been used to inject externally-polarized light into the chip. An auxiliary test structure of a single PBW-based PUC with the same design has also been included for the optical characterization. A tunable laser (ANDO AQ4321D) connected to an

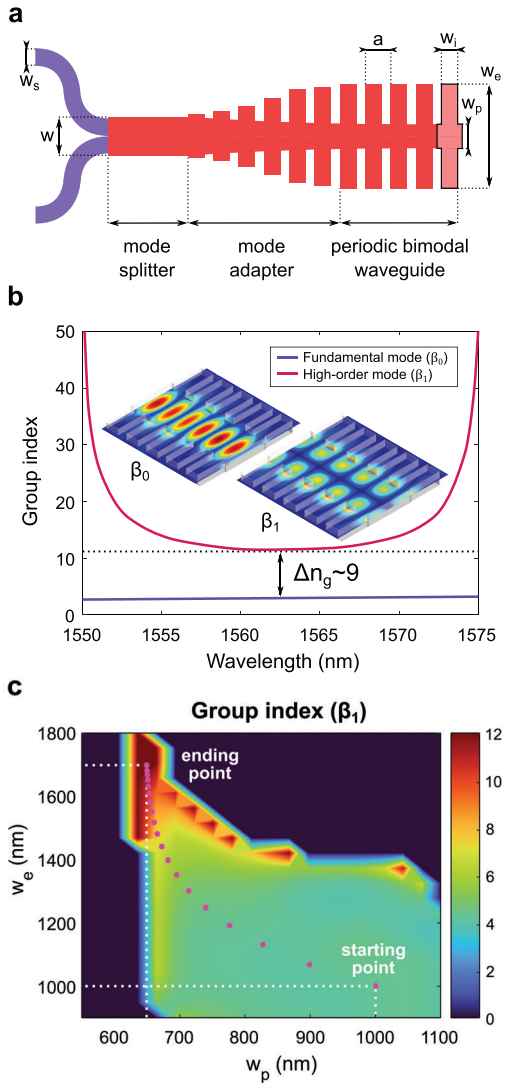

Figure 2. Design and optimization of the PBW-based PUC. a) Schematic of the proposed structure, including the single-mode input ports, the mode splitter and the taper used to adapt the field of the modes to the periodic waveguide. b) Simulated group index as a function of wavelength for both modes β_0 and β_1 supported by the PBW. c) Colormap of the taper optimization as a junction between the uniform and the periodic part. Purple points represents each taper unit dimensions of the mode adapter. The color intensity represents the simulated group index of the periodic unit cell at a central operation wavelength of 1562 nm.

optical spectrum analyzer (ANDO AQ6217C) has been used for the spectral measurements, as well as current sources (Keithley 2401) connected to DC probes to apply electrical power into the heaters.

Figure 3b depicts the static optical response of an isolated PBW structure for both bar and cross ports. An experimental insertion loss and extinction ratio of 0.5 dB and 25 dB are respectively measured, which greatly improves previous results reported for PBWs.[60] It is worth noting that the bandwidth is limited because of the modal dispersion typical of PBWs. Nevertheless, the PBW is designed with a few periods since the shorter the length, the higher the bandwidth.[59] Specifically, the measured bandwidth is 0.62 nm and 3.1 nm for an ER higher than 25 dB and 15 dB, respectively. Figure 3c shows in turn a linear fitting of the insertion losses per PBW-based PUC, measured in the multiport interferometer. Experimental values of 0.49 dB/PUC are obtained, which are in good agreement with the standalone results of Figure 3b. Figure 3d depicts the optical power as a function of the electrical power for bar and cross ports with a measured power consumption P_π of 18 mW. Accordingly, Figure 3e shows the spectral shift of the optical response for a sweep in the electrical power from 0 to 40 mW. A linear spectral shift of 0.4 nmmW^{-1} is experimentally observed. Further experimental measurements regarding the PBW-based PUCs characterization can be found in the supplemental document (see Note S4, Supporting Information).

Experimental demonstrations on the multiport interferometer are carried out using a multi-contact DC probe to simultaneously control the electric power applied to the five PBWs of the circuit. Measurements of 3×3 matrix transformations are depicted in **Figure 4** for an operation wavelength centered at 1590 nm. In this case, PBW_2 and PBW_5 have been configured to bar state by applying an electric power of P_π to them, that is 18 mW. The rest of the PBWs have been left without any electrical power applied, which corresponds to the cross state at the operation wavelength of 1590 nm (see Figure 3b). The normalized spectral results measuring one by one all the possible inputs and outputs configurations of the 3×3 interferometer transfer matrix are shown in Figure 4a. As it can be seen, a 3×3 matrix transformation of real integer coefficients is successfully performed for the default state. A simple calibration of the isolated PBW-based PUC is needed to switch between bar and cross states, however additional electrical control, like chip temperature stabilization, is of great importance in PBW-based circuits as they are highly sensitive to fabrication deviations. Results demonstrate that the fabricated PBW-based PUCs in the multiport interferometer behave similarly to the isolated one, which makes it easy to set up. For example, in order to implement the identity matrix, in Figure 4b an electric power of P_π is applied to the central PBW_3 to switch it to bar state. Similarly, the permutation matrix of Figure 4c is achieved by switching PBW_1 to bar state and the rest left in cross state. More complex matrix implementations are shown in **Figure 5** by including the four optical ports available. Here, 4×4 matrix multiplications are demonstrated by switching the PBWs of the multiport interferometer to implement default and identity matrix transformations, depicted in Figure 5a,b, respectively. Other types of 4×4 matrix multiplications frequently used in quantum processing such as the CNOT and SWAP matrices are also performed in Figure 5c,d by the multiport interferometer. Moreover, power splitting functions can be also programmed in the PBW-based circuit (see **Figure 6**). Matrix transformations of fractional numbers are performed herein with splitting ratios of 1:4, 1:2 and also fractional numbers combined with integer multiplications, Figure 6a,–c, respectively. To achieve such configurations, some of the PBWs have been set to a 50:50 splitting ratio, which corresponds to an electrical power applied of half the P_π, that is 9 mW. In all previously detailed measurements, the insertion losses remain between 1 and 1.5 dB and the extinction ratio is maintained above 20 dB. The experimental results reported here demonstrate the implementation of a PBW-based multiport interferometer for matrix multiplication.

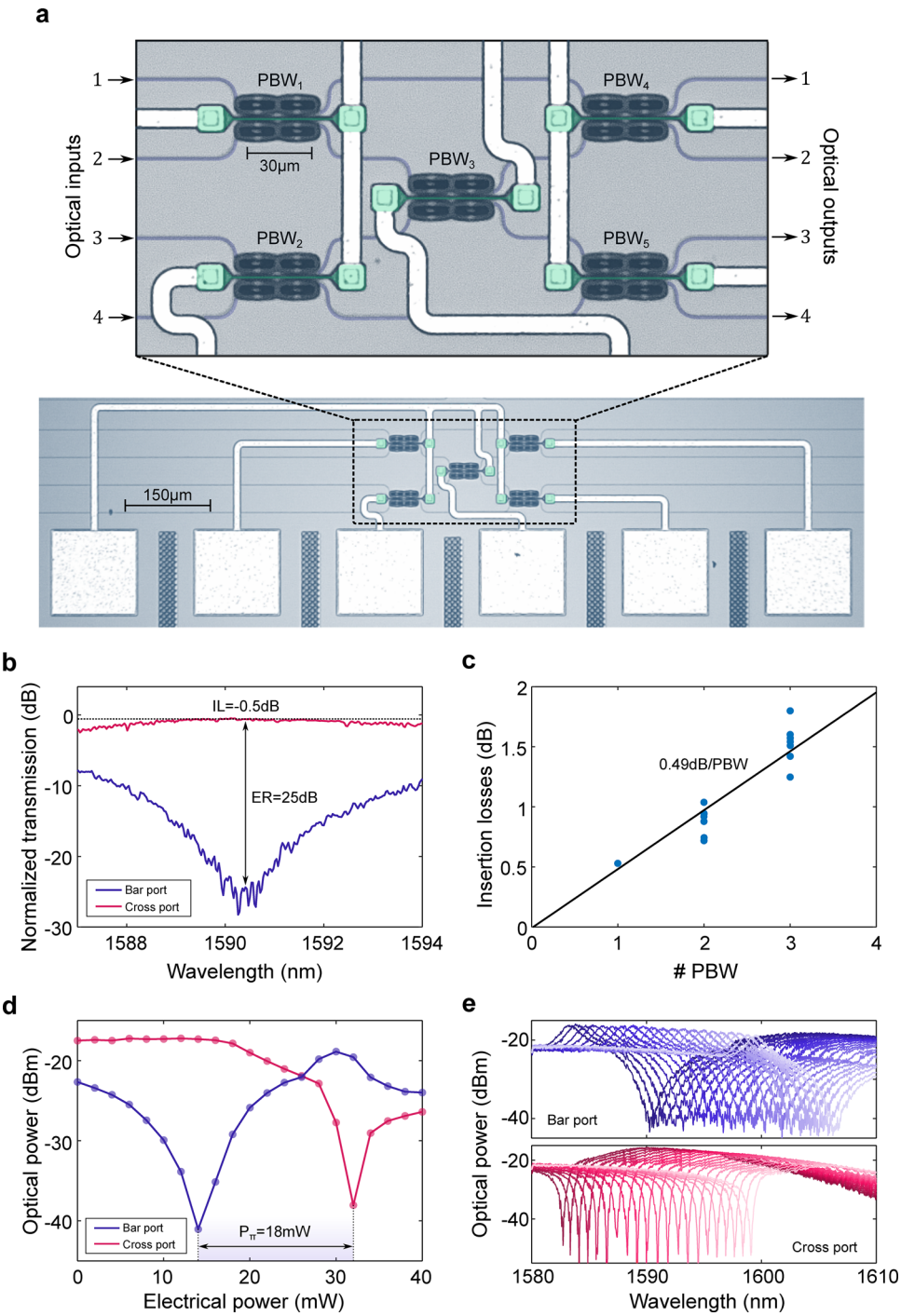

Figure 3. Experimental characterization of the proposed photonic programmable circuits based on PBWs. a) Microscope image of the fabricated photonic chip to implement matrix transformations and a detailed picture of the optical circuit. The 4x4 multiport interferometer footprint dimension is 100×250 μm^2. b) Normalized transmission measurements of an isolated PBW for both bar and cross ports. c) Linear fitting of the measured insertion losses for a different number of PBW-based PUCs in series. d) Optical power of an isolated PBW for different electrical powers applied to the thermo-optic heater at an operation wavelength of 1591 nm. Both cross and bar states are represented. e) Transmitted spectra for a sweep of injected electrical powers from 0 to 40 mW with a step of 2 mW. The spectrum is shifted toward higher wavelengths as the electrical power increases.

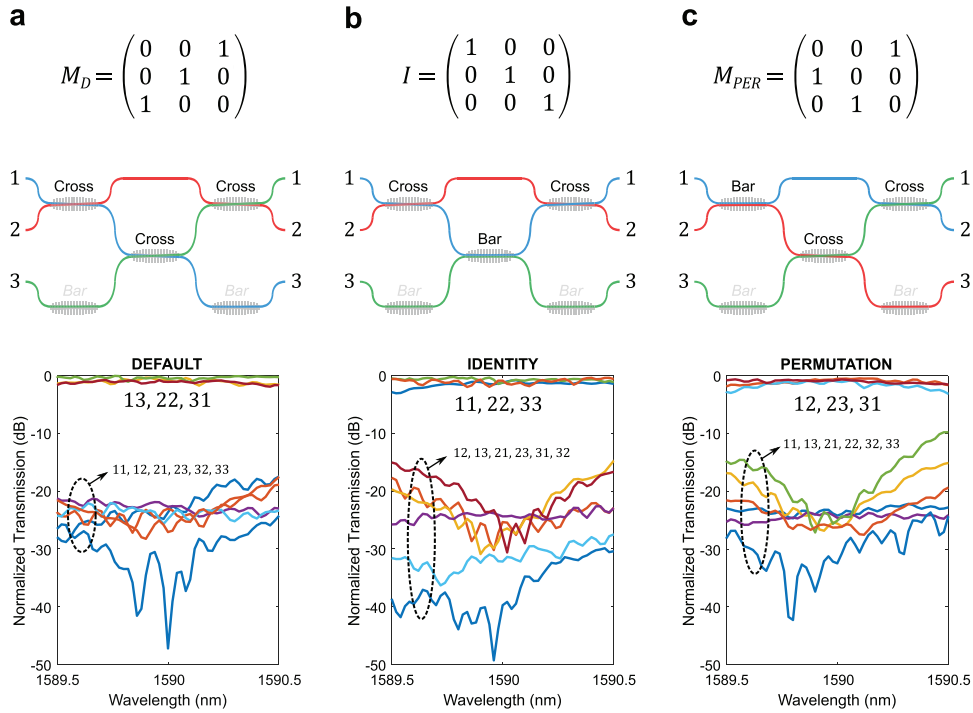

Figure 4. Experimental results of optical 3×3 matrix multiplication using the PBW-based programmable circuit. PBW_2 and PBW_5 have been configured to bar state to implement a rectangular 3×3 multiport interferometer. Circuit configuration and measured normalized transmission spectra in the implementation of the a) default, b) identity, and c) permutation matrices. The results are configured for an operation wavelength of 1590 nm.

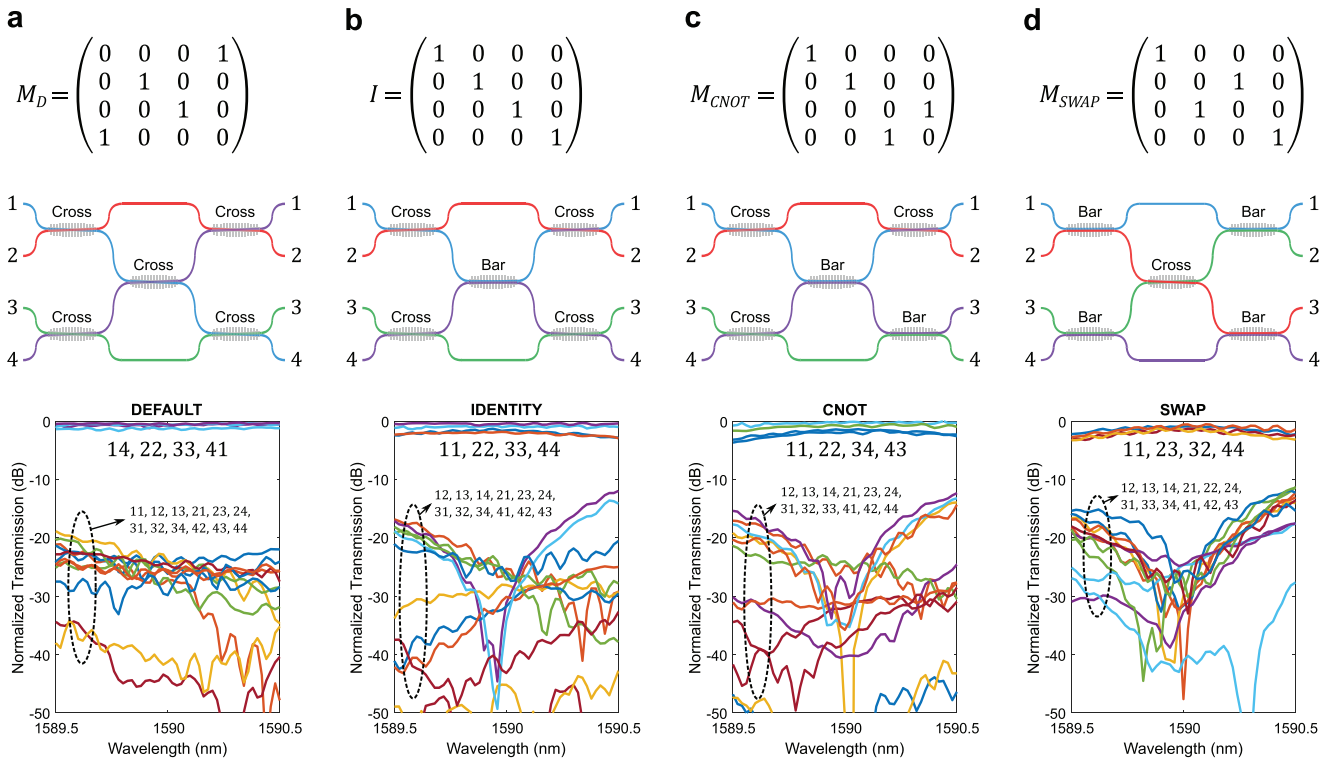

Figure 5. Experimental results of optical 4×4 matrix multiplication using the PBW-based programmable circuit. Circuit configuration and measured normalized transmission spectra in the implementation of the a) default, b) identity, c) C-NOT, and d) SWAP matrices. The results are configured for an operation wavelength of 1590 nm.

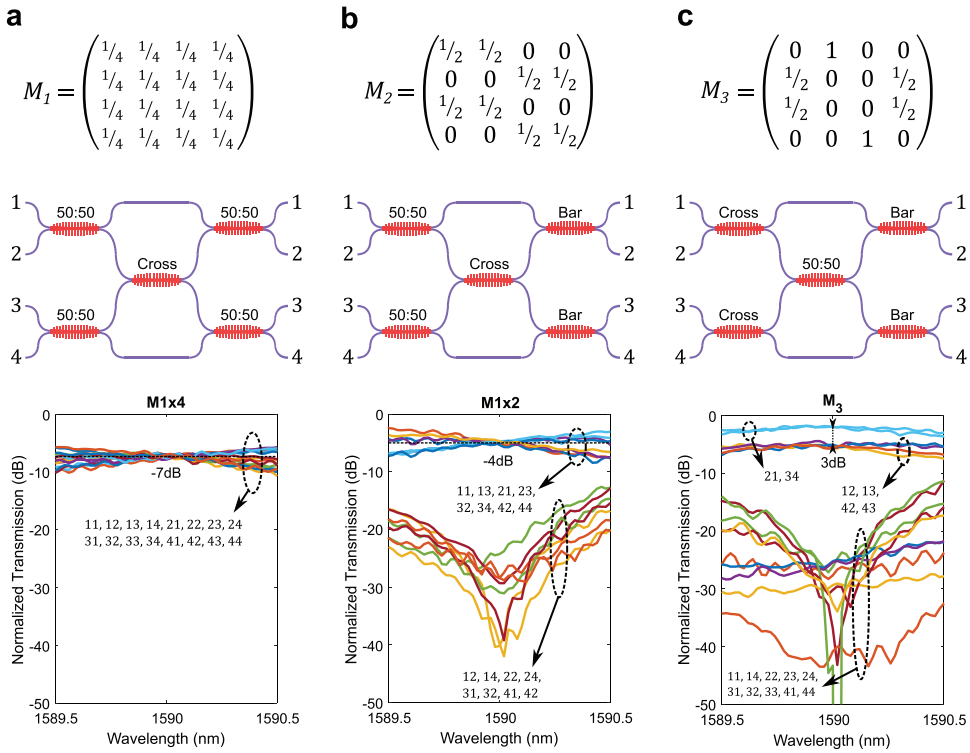

Figure 6. Experimental results of optical 4×4 beam splitting applications using the PBW-based programmable circuit. Circuit configuration and measured normalized transmission spectra in the implementation of different matrices, including a) 1:4 splitting ratio, b) 1:2 splitting ratio, and c) splitting and binary coefficients. The results are configured for an operation wavelength of 1590 nm.

4. Discussion and Conclusion

Experimental results have shown the potential of using PBWs for programmable photonic applications. A novel PUC is presented for such purposes, which comes to strengthen silicon photonics for high-density integration and scalability. These structures can be combined with hybrid integration of other materials such as piezo-electric actuators for high-speed reconfigurability[21] or PCM for non-volatile operation.[40–42] Furthermore, experimental results show improvements in both insertion loss and extinction ratio compared to other similar works on PBWs.[60] Specifically, we demonstrate a loss reduction of 1.5 dB and an extinction ratio increment of almost 10 dB. Further optimization of the mode adapter could be addressed in future work to also reduce reflection, which is key for cascading multiple devices in large-scale programmable PICs. Compared to conventional MZI approaches, the proposed PBW-based PUC presents a more compact structure not only in length but also in lateral size, which is suitable for layout design flattening. However, the resulting operation bandwidth is limited to 1–3 nm, as it occurs with other resonant-based structures as RRs and MDRs.[50,51] PBW-based approaches could be implemented in wavelength division multiplex (WDM) systems to perform several matrix multiplications in parallel. Another thing in common with resonant structures is the need for thermal stabilization as it determines the operation wavelength (see Note S4, Supporting Information). Fabrication tolerances must also be considered when designing periodic structures due to possible deviations produced in the lithography process, and thus device performance degradation (see Note S5, Supporting Information).

A detailed comparison between reported programmable circuits and our work is shown in **Table 1**. The length of most part of the PUCs based on MZI[17,18,24,25] are shrunk more than one order of magnitude by the PBW. It is also worth noting that the lateral size of the proposed PUC is drastically reduced since only one waveguide is used to perform the interferometry, whereas two arms and a vertical separation to avoid cross-talk of at least a few microns are needed in other approaches. As a result, a PUC design area of 30×1.7 μm^2 and a total chip footprint for 4×4 matrix multiplication of 100×250 μm^2 is achieved, which represents an improvement of two-order of magnitude in terms of integration density. Another advantage of the PBW-based programmable circuit is its configuration procedure. In conventional MZI-based circuits, without any applied electric power, the PUC default state is unknown, somewhere in between bar and cross states, so that software control algorithms are needed for self-configuration and stabilization.[26,27] In this work, we shown that all the PBW-based PUCs are in a default cross state for an operation wavelength of 1590 nm, which drastically facilitates the configuration of the circuit. This is due to the very short length of the PBW-based PUC where fabrication errors have almost no influence on its actual state, contrary to what occurs in long MZIs where fabrication roughness significantly affect the default state of the PUC. On the other hand, MDR-based PUCs present similar results in terms of footprint because of their resonant structure,[52] specifically a square shape length of 75 μm and MDR radius of 6.4 μm is

Table 1. Comparison of reported programamble photonic circuits.

Authors	Material platform	Mesh architecture	PUC type	PUC length (um)	Chip size (mm × mm)	Bandwidth (center wavelength)	Power consumption (mW)	Insertion losses (dB)	Functionality
Carolan et al. 2015[17]	Silica	Triangular feedforward	MZI	500	100 × 40	N. D. (808 nm)	400	N. D.	Quantum processing
Zhuang et al. 2015[24]	Si_3N_4	Square recirculating	MZI	3450	3.5 × 8.5	N. D. (N. D.)	~250	N. D.	Radiofrequency applications
Ribeiro et al. 2016[18]	SOI	Triangular feedforward	MZI	500	1 × 3	N. D. (1550 nm)	15	0.9	Beam coupling and switching
Annoni et al. 2017[19]	SOI	Triangular feedforward	MZI	200	3.7 × 1.4	10 nm (1550 nm)	~10	0.25* (estimated)	Mode unscrambling
Pérez et al. 2017[25]	SOI	Hexagonal recirculating	MZI	975	15 × 15	35 nm (1550 nm)	~110	0. 6	Multipurpose
Harris et al. 2017[20]	SOI	Trapezoidal feedforward	MZI	300	2.1 × 4.3	N. D. (1550 nm)	~25* (estimated)	N. D.	Quantum processing
Pérez et al. 2019[23]	Si_3N_4	Triangular recirculating	DD-DC	1278	2.5 × 7.2	N. D. (1550 nm)	350	0.2	Classical processing
Zhang et al. 2020[52]	SOI	Square recirculating	MDR	75	0.4 × 0.4	≈0.5 nm (1550 nm)	2.4	1–9	Classical processing
Tang et al. 2021[48]	SOI	Cascaded feedforward	MDC	≈350	12.2 × 3.6	N. D. (1550 nm)	76	1.3	Matrix multiplication
Pérez et al. 2021[39]	Si_3N_4	Hexagonal recirculating	MZI	1297	5.5 × 11	N. D. (1550 nm)	290	2	Classical processing
This work 2023	SOI	Rectangular feedforward	PBW	30	0.1 × 0.25	3.1 nm (1550 nm)	18	0.5	Matrix multiplication

reported. However, losses in the drop port of the disks are much higher than those reported for the PBW-based circuits, which is not desirable for large-scale integration. Besides, the disk programmable mesh is tailored for signal processing and cannot fully perform matrix operations. In order to implement such unitary transformations, tunable couplers to the disks should be incorporated, which considerably increases the overall footprint.[49]

In conclusion, in this work, we have designed and experimentally demonstrated low-loss highly-compact programmable photonic circuits based on PBWs. The mechanism of the PBW-based PUC and its optimization have been theoretically described. For the experimental realization, we have implemented a rectangular multiport interferometer to perform several 3×3 and 4×4 matrix multiplications including CNOT and SWAP transformations, and also 1:2 and 1:4 beam splitting ratios. The resulting footprint of the proposed device vastly outperforms MZI-based solutions, which represents a step forward toward the realization of large-scale high-density programmable photonic circuits. In general, the results suggest the use of PBW-based programmable chips as a promising alternative with potential application in new emerging fields such as quantum information processing and optical neural networks.

Supporting Information

Supporting Information is available from the Wiley Online Library or from the author.

Acknowledgements

The authors wish to acknowledge the financial support of EIC project 101057934 – INSPIRE.

Conflict of Interest

The authors declare no conflict of interest.

Data Availability Statement

The data that support the findings of this study are available from the corresponding author upon reasonable request.

Keywords

optical matrix multiplications, periodic bimodal waveguides, programmable integrated photonics

Received: June 2, 2023
Revised: August 4, 2023
Published online: September 29, 2023

[1] R. Soref, *IEEE J Sel Top Quantum Electron* **2006**, *12*, 1678.
[2] L. Carroll, J. S. Lee, C. Scarcella, K. Gradkowski, M. Duperron, H. Lu, Y. Zhao, C. Eason, P. Morrissey, M. Rensing, S. Collins, H. Y. Hwang, P. O'Brien, *Appl. Sci. (Switzerland)* **2016**, *6*, 426.

[3] X. Chen, M. M. Milosevic, S. Stanković, S. Reynolds, T. D. Bucio, K. Li, D. J. Thomson, F. Gardes, G. T. Reed, *Proc. IEEE* **2018**, *106*, 2101.
[4] M. Smit, K. Williams, J. V. D. Tol, *APL Photonics* **2019**, *4*, 050901.
[5] D. Melati, A. Alippi, A. Annoni, N. Peserico, A. Melloni, *Opt. Lett.* **2017**, *42*, 342.
[6] M. C. Estevez, M. Alvarez, L. M. Lechuga, *Laser Photonics Rev.* **2012**, *6*, 463.
[7] C. Weimann, M. Lauermann, F. Hoeller, W. Freude, C. Koos, *Opt. Express* **2017**, *25*, 30091.
[8] D. Marpaung, J. Yao, J. Capmany, *Nat. Photonics* **2019**, *13*, 80.
[9] W. Bogaerts, A. Rahim, *IEEE J. Sel. Top. Quantum Electron.* **2020**, *26*, 1.
[10] W. Liu, M. Li, R. S. Guzzon, E. J. Norberg, J. S. Parker, M. Lu, L. A. Coldren, J. Yao, *Nat. Photonics* **2016**, *10*, 190.
[11] J. Capmany, I. Gasulla, D. Pérez, *Nat. Photonics* **2016**, *10*, 6.
[12] D. Pérez, I. Gasulla, J. Capmany, R. A. Soref, *Opt. Express* **2016**, *24*, 12093.
[13] J. Capmany, D. Pérez, *Programmable integrated photonics*, Oxford Univ. Press, Oxford **2020**.
[14] W. Bogaerts, D. Pérez, J. Capmany, D. A. Miller, J. Poon, D. Englund, F. Morichetti, A. Melloni, *Nature* **2020**, *586*, 207.
[15] D. Pérez, I. Gasulla, P. D. Mahapatra, J. Capmany, *Adv. Opt. Photonics* **2020**, *12*, 709.
[16] D. A. B. Miller, *Photonics Res.* **2013**, *1*, 1.
[17] J. Carolan, C. Harrold, C. Sparrow, E. Martín-López, N. J. Russell, J. W. Silverstone, P. J. Shadbolt, N. Matsuda, M. Oguma, M. Itoh, G. D. Marshall, M. G. Thompson, J. C. F. Matthews, T. Hashimoto, J. L. O'brien, A. Laing, *Science* **2015**, *349*, 711.
[18] A. Ribeiro, A. Ruocco, L. Vanacker, W. Bogaerts, *Optica* **2016**, *3*, 1348.
[19] A. Annoni, E. Guglielmi, M. Carminati, G. Ferrari, M. Sampietro, D. A. Miller, A. Melloni, F. Morichetti, *Light: Sci. Appl.* **2017**, *6*, 17110.
[20] N. C. Harris, G. R. Steinbrecher, M. Prabhu, Y. Lahini, J. Mower, D. Bunandar, C. Chen, F. N. Wong, T. Baehr-Jones, M. Hochberg, S. Lloyd, D. Englund, *Nat. Photonics* **2017**, *11*, 447.
[21] M. Dong, G. Clark, A. J. Leenheer, M. Zimmermann, D. Dominguez, A. J. Menssen, D. Heim, G. Gilbert, D. Englund, M. Eichenfield, *Nat. Photonics* **2022**, *16*, 59.
[22] D. Pérez, I. Gasulla, J. Capmany, *Opt. Express* **2018**, *26*, 27265.
[23] D. Pérez-López, A. M. Gutierrez, E. Sánchez, P. DasMahapatra, J. Capmany, *Opt. Express* **2019**, *27*, 38071.
[24] L. Zhuang, C. G. H. Roeloffzen, M. Hoekman, K.-J. Boller, A. J. Lowery, *Optica* **2015**, *2*, 854.
[25] D. Pérez, I. Gasulla, L. Crudgington, D. J. Thomson, A. Z. Khokhar, K. Li, W. Cao, G. Z. Mashanovich, J. Capmany, *Nat. Commun.* **2017**, *8*, 636.
[26] D. Pérez-López, A. López, P. DasMahapatra, J. Capmany, *Nat. Commun.* **2020**, *11*, 6359.
[27] X. Xu, G. Ren, T. Feleppa, X. Liu, A. Boes, A. Mitchell, A. J. Lowery, *Nat. Photonics* **2022**, *16*, 595.
[28] H. Zhou, J. Dong, J. Cheng, W. Dong, C. Huang, Y. Shen, Q. Zhang, M. Gu, C. Qian, H. Chen, Z. Ruan, X. Zhang, *Light: Sci. Appl.* **2022**, *11*, 30.
[29] N. C. Harris, D. Bunandar, M. Pant, G. R. Steinbrecher, J. Mower, M. Prabhu, T. Baehr-Jones, M. Hochberg, D. Englund, *Nanophotonics* **2016**, *5*, 456.
[30] B. J. Shastri, A. N. Tait, T. F. de Lima, W. H. Pernice, H. Bhaskaran, C. D. Wright, P. R. Prucnal, *Nat. Photonics* **2021**, *15*, 102.
[31] Y. Shen, N. C. Harris, S. Skirlo, M. Prabhu, T. Baehr-Jones, M. Hochberg, X. Sun, S. Zhao, H. Larochelle, D. Englund, M. Soljacic, *Nat. Photonics* **2017**, *11*, 441.
[32] F. Ashtiani, A. J. Geers, F. Aflatouni, *Nature* **2022**, *606*, 501.
[33] S. Ohno, R. Tang, K. Toprasertpong, S. Takagi, M. Takenaka, *ACS Photonics* **2022**, *9*, 2614.
[34] M. Reck, A. Zeilinger, H. J. Bernstein, P. Bertani, *Phys. Rev. Lett.* **1994**, *73*, 58.
[35] D. A. B. Miller, *Optica* **2015**, *2*, 747.
[36] W. R. Clements, P. C. Humphreys, B. J. Metcalf, W. S. Kolthammer, I. A. Walsmley, *Optica* **2016**, *3*, 1460.
[37] D. Perez, I. Gasulla, F. J. Fraile, L. Crudgington, D. J. Thomson, A. Z. Khokhar, K. Li, W. Cao, G. Z. Mashanovich, J. Capmany, *Laser Photonics Rev.* **2017**, *11*, 1700219.
[38] A. Macho-Ortiz, D. Pérez-López, J. Capmany, *Laser Photonics Rev.* **2021**, *15*, 2000473.
[39] D. Pérez-López, A. M-Gutierrez, J. Capmany, *Opt. Express* **2021**, *29*, 9043.
[40] M. Delaney, I. Zeimpekis, H. Du, X. Yan, M. Banakar, D. J. Thomson, D. W. Hewak, O. L. Muskens, *Sci. Adv* **2021**, *7*, 3500.
[41] R. Chen, Z. Fang, J. E. Fröch, P. Xu, J. Zheng, A. Majumdar, *ACS Photonics* **2022**, *9*, 2142.
[42] Z. Fang, R. Chen, J. Zheng, A. I. Khan, K. M. Neilson, S. J. Geiger, D. M. Callahan, M. G. Moebius, A. Saxena, M. E. Chen, C. Rios, J. Hu, E. Pop, A. Majumdar, *Nat. Nanotechnol.* **2022**, *17*, 842.
[43] N. M. Estakhri, B. Edwards, N. Engheta, *Science* **2019**, *363*, 1333.
[44] H. H. Zhu, J. Zou, H. Zhang, Y. Z. Shi, S. B. Luo, N. Wang, H. Cai, L. X. Wan, B. Wang, X. D. Jiang, J. Thompson, X. S. Luo, X. H. Zhou, L. M. Xiao, W. Huang, L. Patrick, M. Gu, L. C. Kwek, A. Q. Liu, *Nat. Commun.* **2022**, *13*, 1044.
[45] A. Rahim, T. Spuesens, R. Baets, W. Bogaerts, *Proc. IEEE* **2018**, *106*, 2313.
[46] P. Muñoz, G. Micó, L. A. Bru, D. Pastor, D. Pérez, J. D. Doménech, J. Fernández, R. Baños, B. Gargallo, R. Alemany, A. M. Sánchez, J. M. Cirera, R. Mas, C. Domínguez, *Sensors (Switzerland)* **2017**, *17*, 2088.
[47] R. Tang, T. Tanemura, Y. Nakano, *IEEE Photonics Technol. Lett.* **2017**, *29*, 971.
[48] R. Tang, R. Tanomura, T. Tanemura, Y. Nakano, *ACS Photonics* **2021**, *8*, 2074.
[49] T. Park, Y. Jeong, K. Yu, *Opt. Express* **2021**, *29*, 4645.
[50] R. Soref, *APL Photonics* **2018**, *3*, 021101.
[51] C. Haffner, A. Joerg, M. Doderer, F. Mayor, D. Chelladurai, Y. Fedoryshyn, C. I. Roman, M. Mazur, M. Burla, H. J. Lezec, V. A. Aksyuk, J. Leuthold, *Science* **2019**, *366*, 860.
[52] W. Zhang, J. Yao, *Nat. Commun.* **2020**, *11*, 406.
[53] Y. Meng, Y. Chen, L. Lu, Y. Ding, A. Cusano, J. A. Fan, Q. Hu, K. Wang, Z. Xie, Z. Liu, Y. Yang, Q. Liu, M. Gong, Q. Xiao, S. Sun, M. Zhang, X. Yuan, X. Ni, *Light: Sci. Appl.* **2021**, *10*, 235.
[54] T. F. Krauss, *Nat. Photonics* **2008**, *2*, 448.
[55] T. Baba, *Nat. Photonics* **2008**, *2*, 465.
[56] A. Brimont, J. V. Galán, J. M. Escalante, J. Martí, P. Sanchis, *Opt. Lett.* **2010**, *35*, 2708.
[57] K. E. Zinoviev, A. B. González-Guerrero, C. Domínguez, L. M. Lechuga, *J. Lightwave Technol.* **2011**, *29*, 1926.
[58] L. Torrijos-Morán, B. D. Lisboa, M. Soler, L. M. Lechuga, J. García-Rupérez, *Results Opt.* **2022**, *9*, 100285.
[59] L. Torrijos-Morán, A. Griol, J. García-Rupérez, *Light: Sci. Appl.* **2021**, *10*, 16.
[60] L. Torrijos-Moran, A. Brimont, A. Griol, P. Sanchis, J. Garcia-Ruperez, *J. Lightwave Technol.* **2021**, *39*, 3495.
[61] L. Torrijos-Morán, J. García-Rupérez, *Opt. Express* **2021**, *29*, 33962.